ALICE/98-XX
Internal Note/RIC
September 1998

Development of a pattern recognition method for the HMPID in ALICE (I)

D. Cozza[1], D. Di Bari[1], D. Elia[1], G. Tomasicchio[1],
E. Nappi[1,2], G. Paić[2]

1. Dipartimento Interateneo di Fisica and Sezione INFN, Bari, Italy
2. CERN, Geneva, Switzerland

Abstract

The maximum expected particle density in the HMPID modules (corresponding to an occupancy of about 12%) requires the development of powerful pattern recognition methods for the reconstruction of Cherenkov rings and angles associated to each charged track in ALICE.

In the present note we describe a study performed onto real data taken in ALICE tests at the SPS during the past two years. The method used is based on the Hough transform with a mapping of the pad coordinate space directly to the Cherenkov angle parameter space. The results for the Cherenkov angle resolution obtained by applying the method over data samples with different experimental conditions are reported.

1 Introduction

The hadron identification in the momentum range from 1 to 3 GeV/c (HMPID) in the ALICE experiment at the CERN LHC will be achieved by a single arm RICH detector[1]. A schematic view of the detector is reported in fig.1. It consists of seven 1.3 $\times$ 1.3 m^2 proximity focused RICH modules arranged in a barrel section 4.7 m far from the beam line: details about detector design and technical features can be found elsewhere[2].

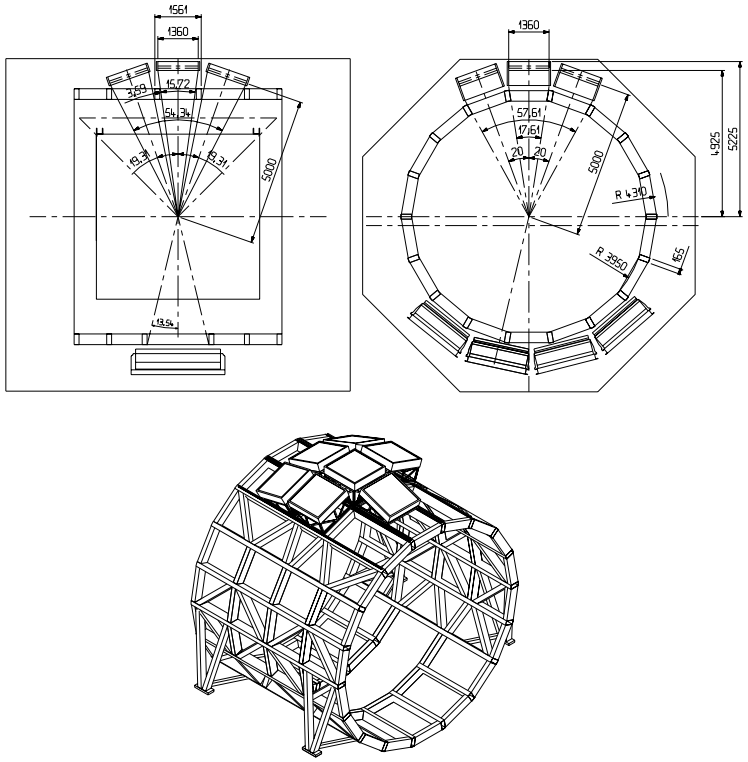

Figure 1: *Axonometric view of the HMPID module layout in ALICE.*

In the acceptance region covered by the RICH (about 5% of the full central) the maximum particle density reaches 100 m^{-2}[3] (including the expected background) with incident angle ranging from 0^o to 15^o. The tracking capability of the ALICE apparatus allows a satisfactory reconstruction of the impact, and of the incident angle for charged particle impinging on HMPID modules[4]. Nevertheless the high global multiplicity onto the photocathodes (track impacts, Cherenkov and feedback photons etc.) and the dependence of Cherenkov images from the tracks incident angle make the pattern recognition and the Cherenkov angle reconstruction very complex.

In the present note we describe the status of a pattern recognition algorithm development for the HMPID. A database of real events collected during the RICH prototype

test and overlapped in such a way as to simulate different high multiplicity environments has been created. A geometrical reconstruction of the photon angles has been developed in order to transform the coordinate space of clusters in the pad plane to a Cherenkov angle parameter space. The interest of this method is that it is very general and valid for any track incidence on the radiator. The signal obtained in this manner has been treated in the frame of a *"Hough-like"* pattern recognition method to determine for each track the corresponding mean Cherenkov angle. The performance of the algorithm has been tested in function of the increasing particle density falling on the RICH surface. The development of the pattern recognition method is of importance because it allows testing the design against specific pattern recognition results obtained. For instance the optimization procedures of parameters like the proximity gap and the radiator thickness may differ for single particles, and for high multiplicity environments.

2 Data sample used for pattern recognition

Different sets of data have been used in the current analysis. The main ones have been obtained as a superposition of single track (beam) events, so that one obtains samples of known densities. The events are obtained by randomly superimposing a fixed number of single ring events on a pad map of the dimensions of the ALICE prototype module. In such a way, sets of respectively 10, 20, 30, 40 and 50 overlapped events per square metre have been formed, the last density being representative of the maximum expected pad occupancy in the ALICE environment. For the time being the results obtained with the superposition of tracks perpendicular to the radiator will be presented, but sets of data with angles of incidence varying from 2.5 to 7.5 degrees are also available and will be analyzed in the near future. Since special care was given to the study of the importance of the photon feedback on the pattern recognition, events measured at different anode voltages (RICH-HV) have been used. In addition, the influence of the "ring" radius has been studied using different gaps. The different samples are summarised in table 1. Another set of data has been obtained from GALICE[5] in order to make a first attempt of analysis over simulated multiple track ALICE events.

Sample	Event type	"ring" radius	Density m^{-2}	RICH-HV
1	340 GeV/c pions (SPS)	155 mm	1, 10, 20, 30, 40, 50	2100 V
2	340 GeV/c pions (SPS)	155 mm	1, 10, 20, 30, 40, 50	2050 V
3	340 GeV/c pions (SPS)	155 mm	1, 10, 20, 30, 40, 50	2000 V
4	340 GeV/c pions (SPS)	122 mm	1, 10, 20, 30, 40, 50	2100 V

Table 1: *Summary of data samples used for the analysis.*

In the fig.2 overlapped events corresponding to the sample (1) are shown for different densities.

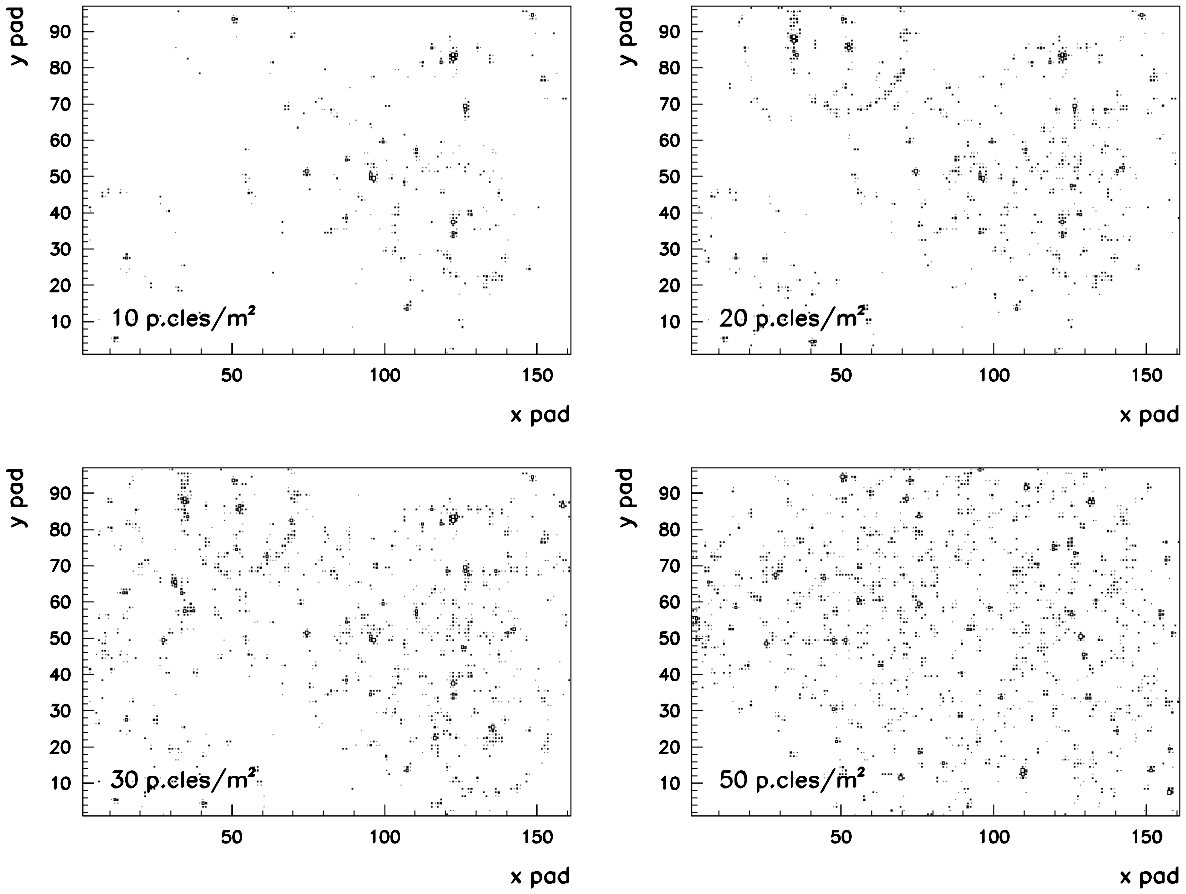

Figure 2: *Overlapped events at different particle densities onto RICH.*

The pad occupancy on the cathode plane depends on the particle density, the ring radius and the HV setting in the RICH chamber: an example of how this quantity scales with these different conditions is reported in fig.3. The fact that the occupancy is higher at smaller radii is understandable in terms of "edge effects". The larger radii get a smaller number of full rings into the detector active area than is the case for smaller radii.

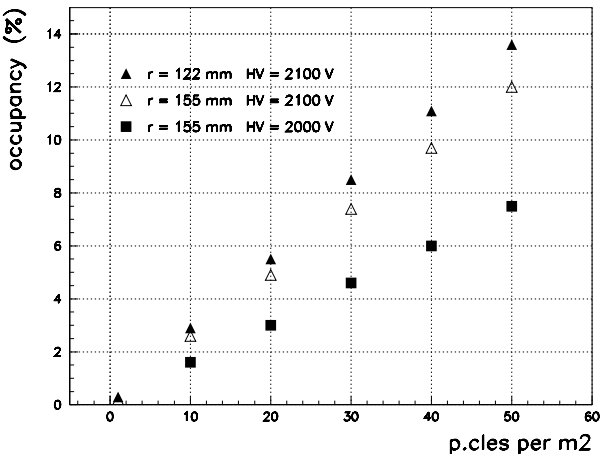

Figure 3: *Occupancy on the photocathode at different gap size and anode voltage.*

3 The signal from the HMPID readout: the pad hit and the clusters

The signal recorded by the pad readout of the MWPC consists of the information on:

- the coordinates of the pads where a signal (after zero suppression) has been recorded: we call these *"hit pads"*;
- the amount of charge induced on each hit pad, obtained by the analog readout scheme of the electronics.

Due to the nature of the induction process (the characteristic spread), the pad size (8 $\times$ 8.4 mm^2), and the fluctuation of the charge in the avalanche, the signal produced by a single track ionization in the gas or by Cherenkov photons converted in the CsI layer on the cathode will result in a "cluster" the size of which may vary from one to several pads.

4 Cluster centroids and deconvolution

The map of hit pads is first analyzed for clusters by a cluster finding algorithm that recognizes, as such, groups of adjacent hit pads that share at least one common edge. In a second pass, the identified clusters are analyzed for the existence of possible multiple charge maxima in a single cluster, indicating that the recognized cluster represents, in fact, an overlap of two or more clusters. In cases where multiple maxima are observed, a deconvolution algorithm is applied resulting in so-called "resolved clusters". Finally,

a charge-weighted centroid is defined for each identified resolved cluster. Although this procedure allows a better localization of the photons, it does not mean that clustering can be usefully applied in high occupancy environments: this point will be addressed in Section 7.

5 Reconstruction of the "Cherenkov signal"

In the most general case of multiple tracks on the HMPID we will be confronted to:

- a large–sized map of hits with a very complex pattern where individual RICH patterns can hardly be identified by eye (see fig.2);
- a map of "impacts" of tracks as extrapolated from the TPC to the HMPID cathode plane;
- a number of real impact corresponding to large charge clusters closest to the extrapolated impact points[4].

To extract from the described cluster distribution and track impact information the Cherenkov signal for a chosen track we proceed as follows:

- we define a *"fiducial zone"* on the detector plane where the Cherenkov photon clusters emitted by the chosen track of known momentum and incidence angle are observed;
- we associate to each cluster in the fiducial area a "Cherenkov angle" of emission in the radiator as if it were produced by the track — a method originally proposed in [6].

The latter task is performed using a backtracing algorithm described in the next section.

5.1 Geometrical backtracing

The backtracing means that from any cluster (or pad) centroid we try to reconstruct the angle under which the photon causing it could have been emitted had it belonged to the chosen track. To be able to start backtracing we have to make the following assumptions:

1. the origin of 'photons' resulting in the same reconstructed angle is chosen to be one point on the track path through the radiator. The z coordinate of this point (see fig.4) varies, although only slightly, with angle (because of the absorption in the radiator), and is close to the middle of the radiator thickness on the track path as described in more details later;

2. all the 'photons' are assumed to be of the same energy corresponding to the mean energy of the photons producing photoelectrons in the HMPID RICH, i.e. 6.85 eV;

3. no assumption is made on the β of the particle.

The reference system has the origin origin at the entrance point of the Minimum Ionizing Particle (MIP) in the detector, as illustrated in fig.4, we define:

(x_p,y_p) = MIP impact coordinates onto the photocathode
(θ_p,ϕ_p) = MIP polar and azimuthal angles
(x,y) = photon impact coordinates onto the photocathode
(θ,ϕ) = photon polar and azimuthal angles
r_w, q_w, t_{gap} = radiator, quartz and gap widths
n_f, n_q, n_g = freon, quartz and methane refraction indices.

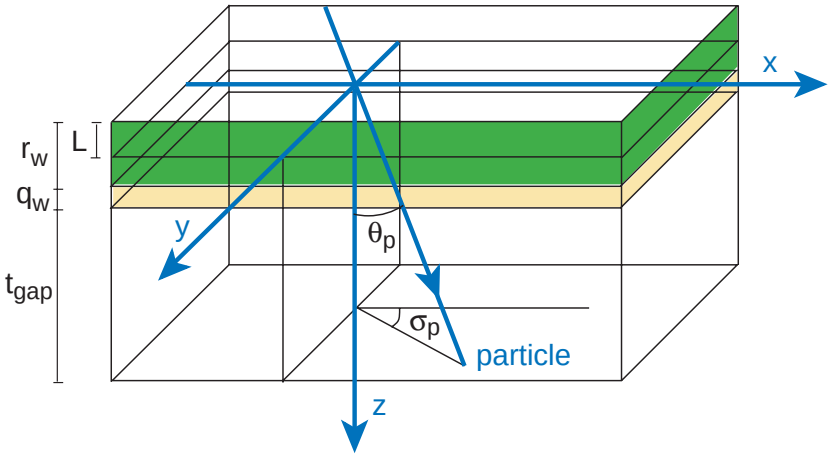

Figure 4: *Reference system used in the backtracing.*

The azimuthal angle ϕ for the photon can be evaluated, for the first iteration, assuming an average emission depth L (at the middle of the radiator):

$$tan\phi = \frac{y - Ltan\theta_p sin\phi_p}{x - Ltan\theta_p cos\phi_p} \tag{1}$$

Using this value of ϕ and defining a and R as

$a = [(r_w\text{-}L) + q_w + t_{gap}]\tan\theta_p$

$R =$ *distance MIP-photon cluster on the photocathode*

the following equation has to be solved:

$$R^2 = [acos\phi_p - bcos\phi]^2 + [asin\phi_p - bsin\phi]^2 \tag{2}$$

In the equation (2) b is a function of the polar angle of the photon according to

$$b = (r_w - L)tan\theta + q_w \frac{n_f sin\theta}{\sqrt{n_q^2 - n_f^2 sin^2\theta}} + t_{gap} \frac{n_f sin\theta}{\sqrt{n_g^2 - n_f^2 sin^2\theta}} \tag{3}$$

Therefore the solution of the Equ.(2) taking into account the (3) provides the value of θ for the current photon of the MIP.

The emission point L, is evaluated per each photon, with an iterative procedure: at the first iteration L is the middle of the radiator width (0.5 cm) then a corresponding value of θ is extracted. With this value the most probable emission point L(θ) is evaluated as follows. The mean emission distance of photons is given by

$$\langle l_p \rangle = \frac{\int_0^{\frac{r_w}{\cos\theta_p}} l_p T(l_{ph}) dl_p}{\int_0^{\frac{r_w}{\cos\theta_p}} T(l_{ph}) dl_p} \tag{4}$$

where $T(l_{ph})$ is the transmission coefficient of the freon along the photon path (l_{ph}) in the radiator. This path length is given by

$$l_{ph} = l_p \frac{\cos\theta_p}{\cos\theta} \tag{5}$$

so the transmission takes the form

$$T(l_{ph}) = e^{-l_{ph}/l_{abs}} \tag{6}$$

In the equation (6) l_{abs} is the photon absorption length in the freon, given by (-1.8/lnT_o) cm: for 6.85 eV photon energy, T_o for 1.8 cm of freon is ≈ 0.88.

The projection of l_p onto the normal to the detector gives the average emission length (the most probable one for the current photon), i.e.

$$\langle L \rangle = r_w - \langle l_p \rangle \cos\theta_p = r_w - l_{abs}\cos\theta + r_w \frac{e^{-\frac{r_w}{l_{abs}\cos\theta}}}{1 - e^{-\frac{r_w}{l_{abs}\cos\theta}}} \tag{7}$$

By using this value as L in the equ.(1), again θ is calculated: the same procedure has been iterated until convergence is reached.

Finally the Cherenkov angle η_c for the photon is calculated by:

$$cos\eta_c = sin\theta_p cos(\phi - \phi_p) + cos\theta_p cos\theta \tag{8}$$

6 Analysis of single beam events

As a first step in the analysis procedure single beam events at the SPS have been processed in order to obtain the Cherenkov angle resolution in absence of background coming from other tracks. In fig.5(a) the distribution of extracted Cherenkov angles per cluster, using the described method, is shown for the data set (1): there is a clear signal with negligible background. The gaussian fit of the distribution gives a $\sigma_{\eta_c} \approx 12.8$ mrad.

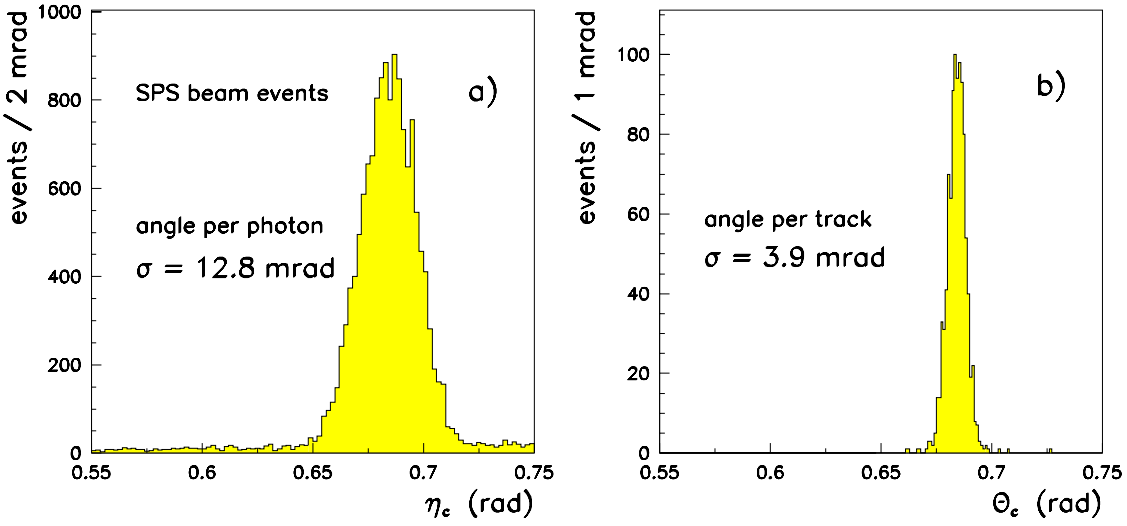

Figure 5: *Photon angle distribution (a) and track Cherenkov angle distribution (b) for beam events at SPS in sample (1).*

By averaging the η_c for all the photons, the Cherenkov angle per track θ_c is obtained: the distribution, shown in fig.5(b), indicates this resolution to be 3.9 mrad. The distribu-

tion in fig.5(b) has been obtained considering only photons with η_c angle ranging between 0.550 and 0.750 rad.

To determine the baseline parameters we show, in fig.6 the resolved cluster multiplicity, the cluster size and charge spectrum for the case of single event patterns.

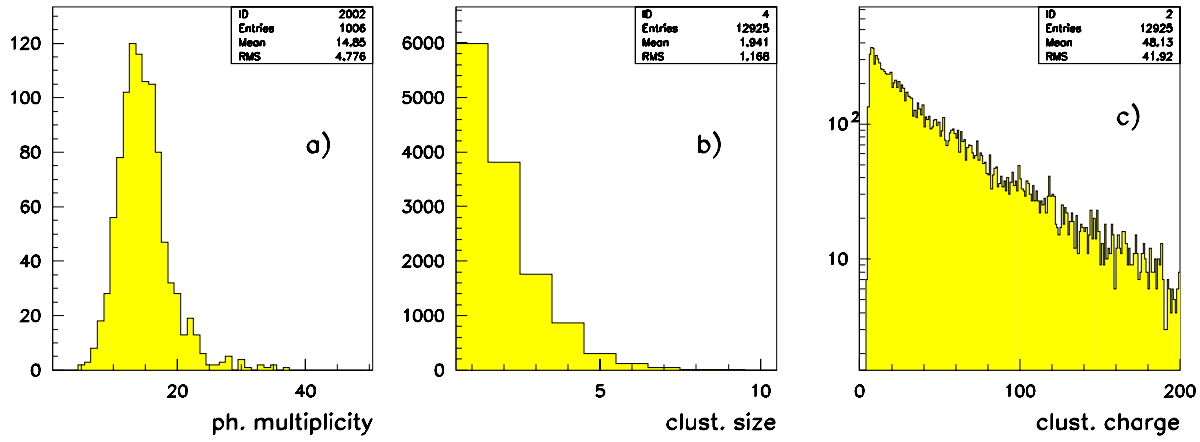

Figure 6: *Photon cluster multiplicity (a), cluster size (b) and charge (c) in sample (1).*

7 Analysis of overlapped data sets

Although at first sight it seems advantageous to use the cluster centroid method in the backtracing for better localization we have observed that the use of the clustering procedure on the hit pads, in case of multiple particle events leads to a clear signal reduction per MIP. Moreover the clustering procedure in high density events modifies the topological (ring) reconstruction since it can merge together different photon contributions in a single cluster with a biased centroid location.

It has been observed that the modification of the global pattern in high multiplicity environments, if treated in terms of a global clustering, reduces in an appreciable way the signal over background ratio in the η_c distribution. For this reason we have analyzed the multi-ring events taking into account only the hit pads, assuming as photon-pad location the middle of the pad itself.

7.1 Fiducial region

Moving to the analysis of "multi-ring" events, the backtracing algorithm described in section 5.1 has to be applied to all photon-pads for every MIP in the event. Starting

from the MIP position and knowing detector parameters, a wide fiducial region around the MIP impact where all photons relevant to the track could eventually be found.

The analysis program takes into account the previous considerations, essentially by calculating for each MIP in the event the corresponding fiducial region: in the case of zero incident angle particle, this region is a circular band. In the present analysis we have chosen to backtrace all pad hits corresponding to photon angles between 0.550 and 0.750 rad.

For instance we can see in fig.7(a) the map of all backtraced photons (the MIP impact position is always the origin), i.e. the fiducial band assumed: the picture corresponds to a density of 10 particles m^{-2} for sample (1).

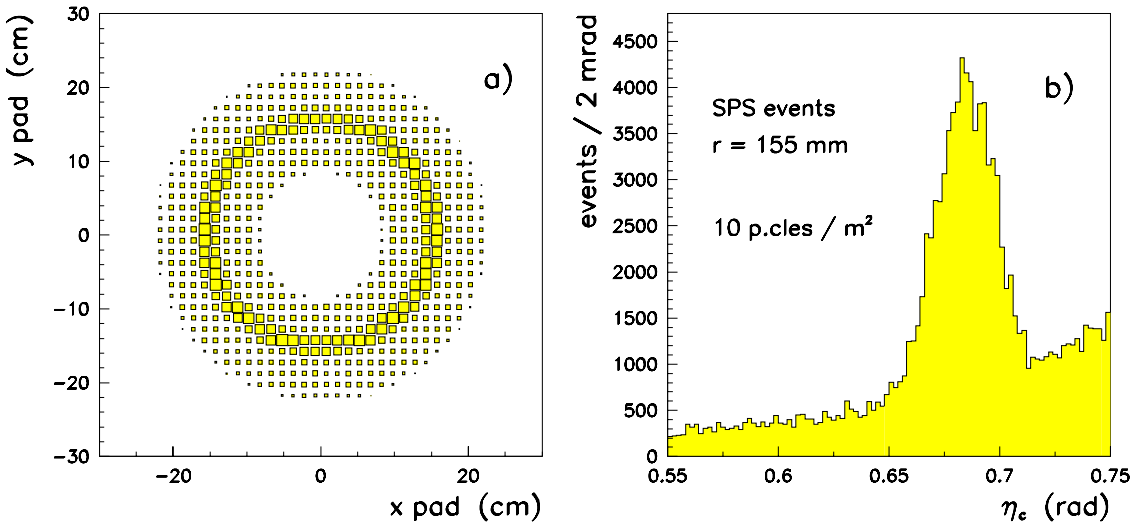

Figure 7: *Fiducial band around the MIP (a) and photon angle distribution (b) at 10 particles m^{-2} for sample (1).*

The η_c distribution in fig.7(b) shows now two distinct components: the peak around the Cherenkov angle produced by photons belonging to the tracks analyzed, and a continuous background belonging to photon-pads produced by other tracks and falling in the fiducial zone analyzed. The increasing profile of the background distribution is expected and is mainly due to the fact that at larger η_c values a larger surface of the plane is covered for equal η_c bins: this surface scales as $[\tan\eta_c(1+\tan^2\eta_c)]$.

This distribution is the challenge to the pattern recognition, namely to determine, in cases when a strong background is present under the true photon peak, per each track the position of the maximum of the photon distribution per track. The rising contribution of the background at larger angles will bias in any pattern recognition the results towards

higher angle. Therefore before applying a pattern recognition algorithm we have to find ways to treat the background.

7.2 Treatment of the background

The background has been parameterised with an analytical form:

$$F_{bkg}(\eta_c) = [\tan\eta_c(1+\tan^2\eta_c)]^{\alpha} + A + B\tan\eta_c, \tag{9}$$

where α = 5.52, A = -7.80 and B = 22.02. This parametrisation fits equally well all the studied densities.

With this analytical form each photon-pad has been weighted according the following procedure. For each analyzed track (MIP impact) the corresponding η_c distribution is calculated. In this distribution we calculate the number of photon-pads N_{bkg} in a sampling band far from the signal (i.e. with η_c between $\eta^1_{bkg} = 0.720$ and $\eta^2_{bkg} = 0.760$ rad).

So the expected amount of background photon-pads at any η_c can be estimated by means of the (9), as

$$R_{bkg}(\eta_c)d\eta_c = \frac{F_{bkg}(\eta_c)N_{bkg}}{\int_{\eta^1_{bkg}}^{\eta^2_{bkg}} F_{bkg}(\eta'_c)d\eta'_c}d\eta_c \tag{10}$$

In the equ.(10) $d\eta_c$ is 1 mrad: it means that $R_{bkg}(\eta_c)d\eta_c$ is the expected amount of background photons in 1 mrad bin at the angle η_c. It is clearly shown in the fig.8 the good agreement of this estimated background (dashed line) with the background shape at all particle densities. The white distribution in each case corresponds to the photon-pad η_c spectrum obtained for all analyzed MIPs.

If $N_{ph}(\eta_c)d\eta_c$ is the η_c spectrum for the MIP under study, to take into account the background, each photon in each bin should be weighted by

$$W_{bkg}(\eta_c) = 1 - \frac{R_{bkg}(\eta_c)}{N_{ph}(\eta_c)} \tag{11}$$

The dark distributions in fig.8 have been obtained by entering each photon with the corresponding weight calculated by (11). In this way the background contribution has been taken into account so that, *a priori*, no systematic biasing of the signal will occur in the pattern recognition.

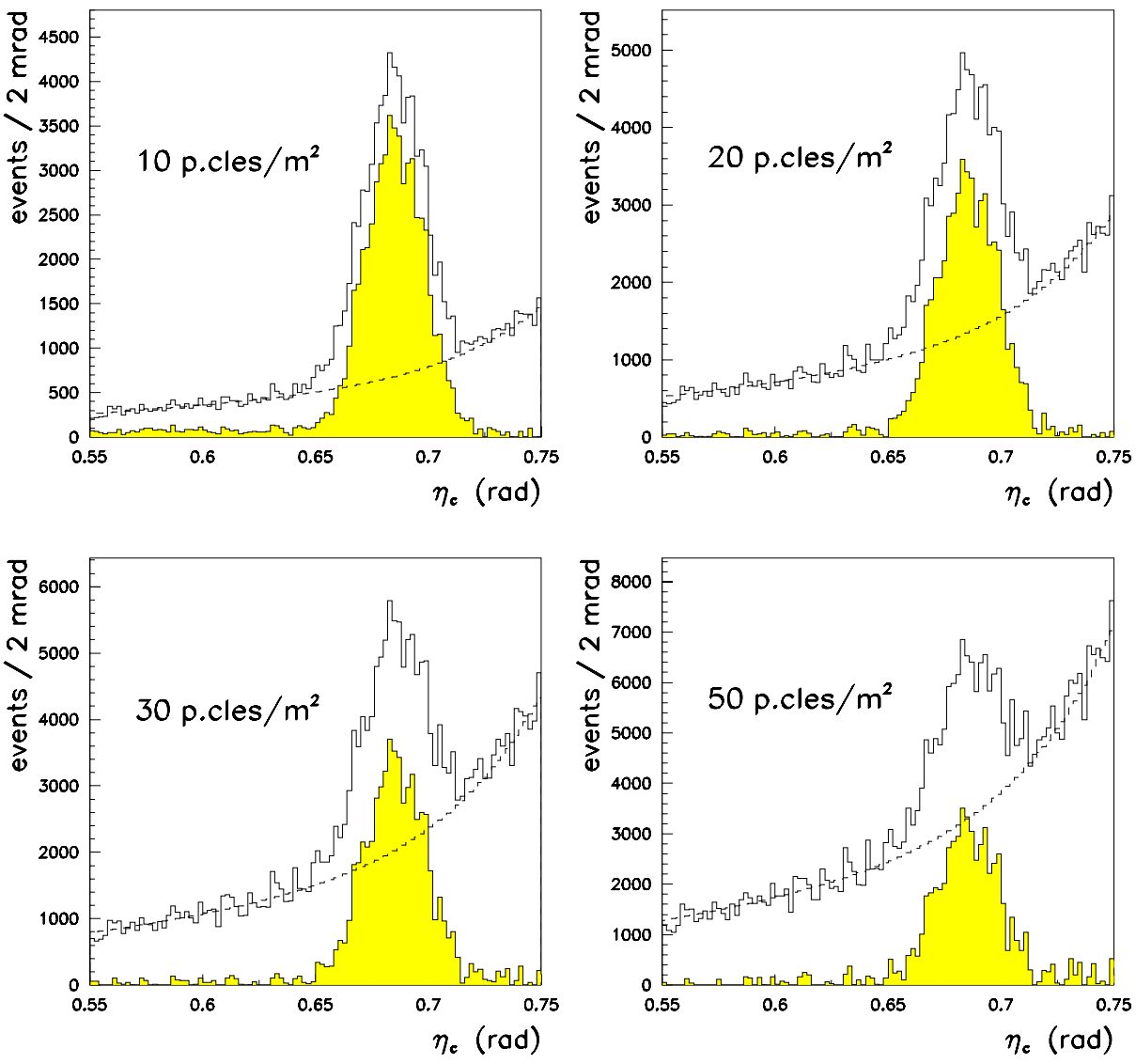

Figure 8: *Distributions of η_c per photon-pad at different particle densities, with estimated background (dashed) and after background subtraction (dark) for sample (1).*

7.3 Extraction of the mean Cherenkov angle

The determination of the mean Cherenkov angle for all the photons associated to a track is the goal of the pattern recognition. The η_c signal observed in fig.8 shows that there is no drastic deterioration of the width of the signal distribution, but the mean Cherenkov angle is influenced by the presence of the background signal. In the following we will describe in details the applied method that relies on the Hough transform method modified to accommodate the fact that the signal has a natural width. Of course the signal seen

on a single event is rather small as shown in the fig.9 requiring a very complex analysis to extract the mean Cherenkov angle. We have adopted the so-called sliding window approach that will be described in detail later but consists in sliding a window of a width comparable to the width of the signal in η_c over the spectrum. At each step in the sliding, the number of pads found within the window is counted, the position of the maximum recorded allowing after iterative averaging procedures for the extraction of the mean angle.

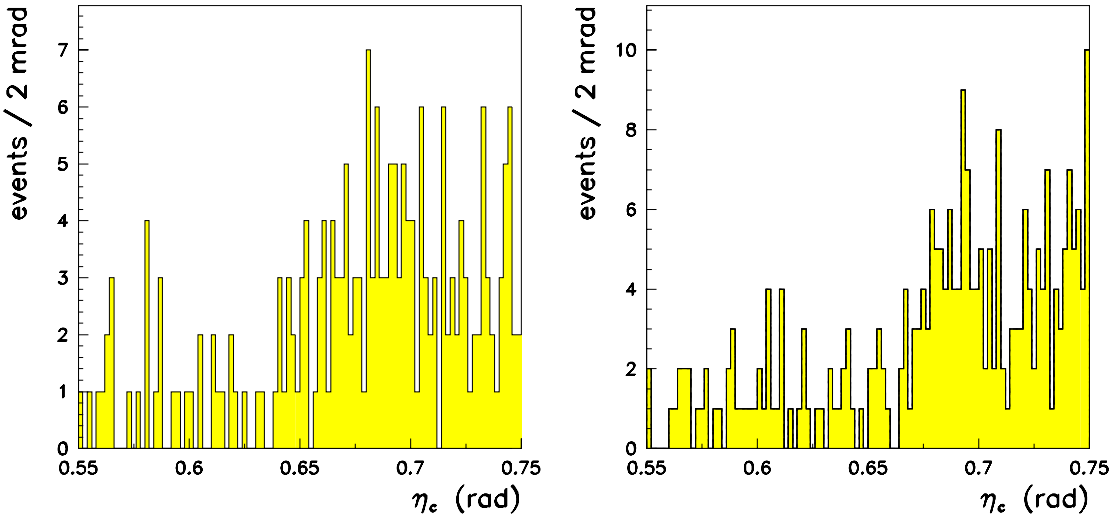

Figure 9: *Distributions of η_c per photon-pad for single MIPs in sample (1) at 50 particles m^{-2}.*

In the following we will shortly review the steps in the pattern recognition that we have developed. Our basic approach is to apply a Hough transform method which has been modified to accomodate the fact that the signal in the η_c coordinate has an intrinsic width. To account for that width we apply a *sampling band* approach that consists in sliding a window of a width comparable to the width of the signal over the η_c spectrum. At each step in the sliding, the number of pads found within the window is counted. When the window reaches the region for which the number of counted photon-pads is the largest, the content of the window is called *Hough selected photon-pads*. Using that information and the known background weights, an iterative procedure is used to finally determine the value of the mean Cherenkov angle associated to that track.

7.3.1 The Hough Transform Method

The pattern recognition for the HMPID, on the track level, has been implemented using the Hough transform technique to extract the mean Cherenkov angle per track as a

parameter to be estimated in a transformed parametric space[7,8]].

The Hough Transform method (HT) is an efficient implementation of a generalized *template matching* strategy for detecting complex patterns in binary images. This is achieved by analysing the parameters which characterize these patterns and looking for local maxima in a *feature parameter space*[9]. The main advantage of the Hough transform is that it is relatively unaffected by topological gaps in curves and by high noise background in spot-like images[10]. Let us assume that we transform a Cartesian space in a feature space:

$$\mathbf{x} \rightarrow (\mathbf{a}, T(\mathbf{x}, \mathbf{a})) \tag{12}$$

where $\mathbf{a}$ is a parameter vector and T($\mathbf{x}$,$\mathbf{a}$) its relative transform. For each thresholded contribution of T($\mathbf{x}$,$\mathbf{a}$) in the parameter space, a Hough counting takes place in the so called *'Hough Counting Space'* (HCS):

$$HCS(T(\mathbf{x}, \mathbf{a})) := HCS(T(\mathbf{x}, \mathbf{a})) + w \tag{13}$$

where w is a given weight to be assigned to the *feature vector* $\mathbf{a}$ which, in the simplest case, is assumed unitary. The *incrementation strategy* of equation (13) can be refined further by applying an incrementation function:

$$w = w(\mathbf{x}, \mathbf{a}) \tag{14}$$

which implements a weighting policy in such a way to use other relevant information associated with a given feature point [11]. The Hough estimator for the feature vector is given by the bin value in HCS which provide the highest occurrence in the parameter space.

For the HMPID analysis we have

$$(x, y) \rightarrow ((x_p, y_p, \theta_p, \phi_p), \eta_c), \tag{15}$$

If we assume $\mathbf{a} = (x_p,y_p,\theta_p,\phi_p)$ to be already known, the transform will reduce the problem to a solution in a one-dimensional mapping space. The HCS in this case represents the photon Cherenkov angle η_c spectrum and, indeed, a Hough estimator for the Cherenkov angle θ_c of the particle is chosen as the highest peak provided by all the photons wich fall in that angle bin. Thus, the HCS accumulates the contributions from several Cherenkov photons according the expression (13). The analysis procedure can be easily extended and made more effective if the weight function (14) is used to take into

account other factors like the background evaluation or the charge contribution for each Cherenkov photon.

The transformation which provides the parameter η_c for a given **a** vector has been already described in the section 5.1 as the *geometrical backtracing algorithm* to extract the Cherenkov angle associated to each photon pad. Each MIP cluster is excluded from this transformation and for each MIP cluster a scanning in the *MIP reference system* is done in such a way to get the η_c values ranging from 0.550 to 0.750 rad. It should be noted that this kind of approach allows to be independent from the topological shape and size of the specific Cherenkov pattern cut in the plane of the detector (i.e. circular, elliptic, parabolic). This is due to the fact that the particle identification happens in the Cherenkov photon angle space, instead of the Cartesian one (see fig.10).

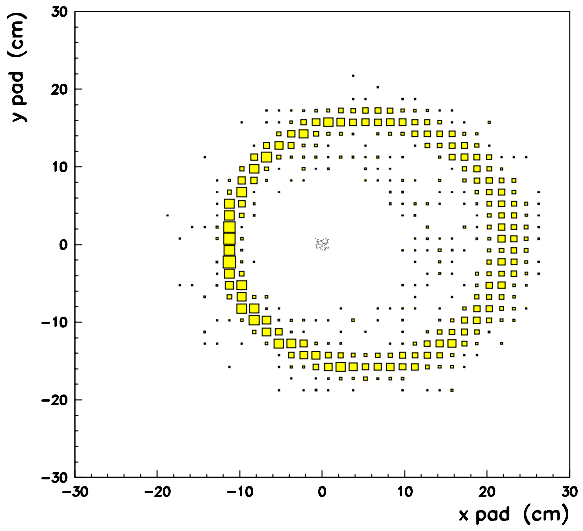

Figure 10: *Fiducial band around the MIP at 10 particles m^{-2} and 5^o incidence angle.*

7.3.2 The HT method modified with correlation bands

The basic HT method applied for the HMPID has been enhanced in such a way to be less influenced from the background caused from several noise sources[12].

For each photon there is a spread in the Cherenkov angle to be taken into account, which makes harder to achieve a good resolution σ_{η_c} in the Cherenkov angle identification. In order to enhance statistically as much as possible the signal in the η_c spectrum, the incrementation expression (13) has been modified as described in the following.

The following integration in the η_c space over a *'sampling band' b* has been applied:

$$HCS'(\eta_c) = \int_{\eta_c - \frac{b}{2}}^{\eta_c + \frac{b}{2}} HCS(\eta'_c) d\eta'_c \tag{16}$$

which in the discrete case, where $d\eta_c = 1$ mrad (i.e. $\eta_c(k) = k\ d\eta_c$, k integer), transforms into the correlation:

$$HCS'(\eta_c(k)) = \sum_{i=\eta_c(k)-\frac{b}{2}}^{\eta_c(k)+\frac{b}{2}} HCS(i) \tag{17}$$

The HCS has been calculated using $w = W_{bkg}(\eta_c)$ defined defined by Equ.(14) as the incrementation function. The sampling band in the correlation has been determined at 40 mrad for the smallest σ_{η_c} value.

8 Results obtained with SPS overlapped data

The first output response of the Hough analysis procedure, per each MIP, is a θ_c^{Hough} value for the Cherenkov angle: this value corresponds to the centre of the most populated correlation band (*Hough selected band*), in the sense previously specified. In fig.11 the distributions of θ_c^{Hough} are shown at three different particle densities: there is a clear degrading of the σ_{θ_c} at increasing density and also the shape of the distributions are not well gaussian shaped. In fig.11 σ_{θ_c} ranges from 5.1 to 8.0 mrad, respectively moving from 10 to 50 particles m^{-2} in the sample (1).

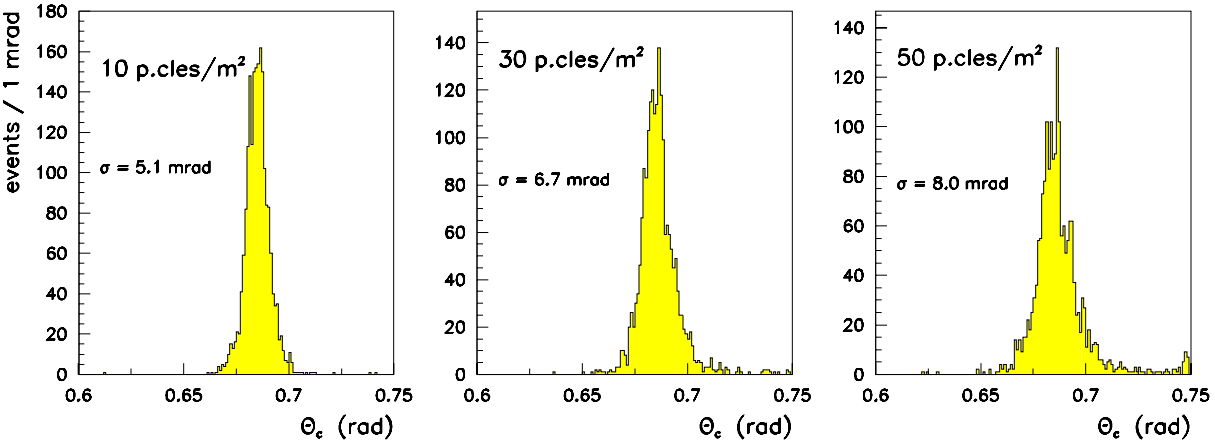

Figure 11: *Hough angle distributions at different particle densities for sample(1).*

The second information, per each analyzed MIP, that can be extracted from the pattern recognition is the photon–pads falling into the Hough selected band: we call those

"Hough selected photon-pads" and their number will be indicated by N_{ph}^{Hough}. In fig.12(a) these selected photon-pads are shown in the case of $10/m^2$ particle density. In fig.12(b) the evolution of the N_{ph}^{Hough} distribution with the particle density is also reported: the three plots superimposed refer to samples with equal total number of MIPs.

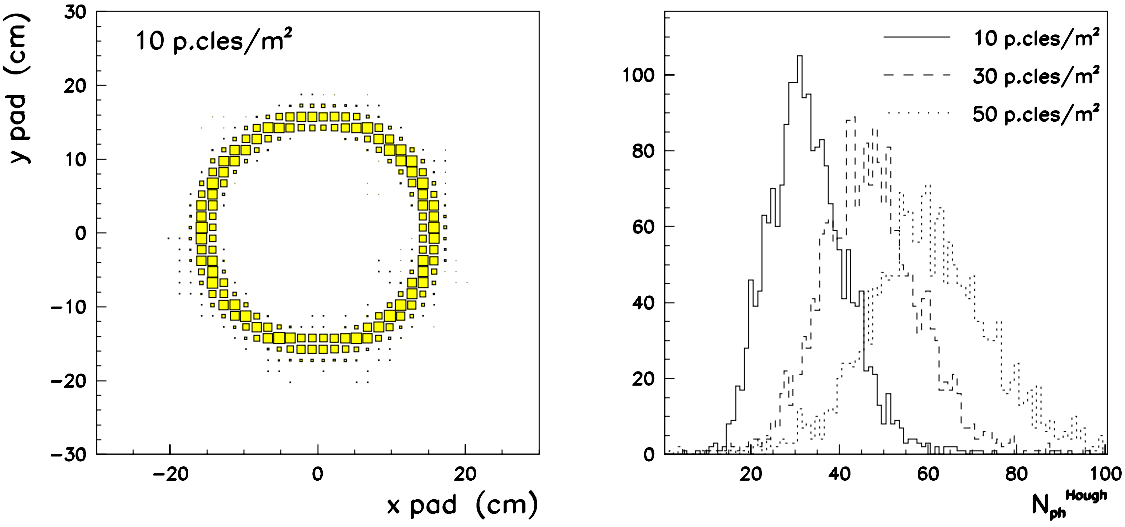

Figure 12: *Hough selected photon-pads at 10 particles m^{-2} and multiplicity distributions at different densities for sample (1).*

In the pattern recognition the band selection performed by the Hough method, as described in section 7.3.1, takes into account the background: this determines θ_c^{Hough} and N_{ph}^{Hough}. Beyond that other outputs may be used to achieve the final response for the mean Cherenkov angle. These consist of the different η_c angles for the *Hough selected photon-pads* and their background related weights. The pattern recognition provides this final output:

$$\theta_c^{Hough} \qquad N_{ph}^{Hough} \qquad (\ \eta_c(i),\ W_{bkg}(\eta_c(i)), \qquad \mathrm{i} = 1,\ N_{ph}^{Hough}\ )$$

This information can be used to provide a better estimation for the MIP Cherenkov angle. Further, an averaging can be satisfactorily used over the selected photon-pads only, by using their angles with the corresponding background weights. The applied method makes the calculation of the averaged weighted angle as:

$$\langle\theta_c\rangle = \frac{1}{W_{tot}} \sum_{i=1}^{N_{ph}^{Hough}} W_{bkg}(\eta_c(i))\eta_c(i) \qquad W_{tot} = \sum_{i=1}^{N_{ph}^{Hough}} W_{bkg}(\eta_c(i)) \tag{18}$$

and the calculation is iterated, discarding photon-pads with η_c out of a defined number of sigmas from the $\langle\theta_c\rangle$ value. Finally, by iteration the best estimate for the current MIP

angle θ_c^{MIP} is obtained.

In fig.13 the θ_c^{MIP} distributions at three different densities are shown, with the bottom right plot resuming (white triangles) the behaviour of the corresponding sigmas (*"angle resolution"* per MIP) versus the particle density itself.

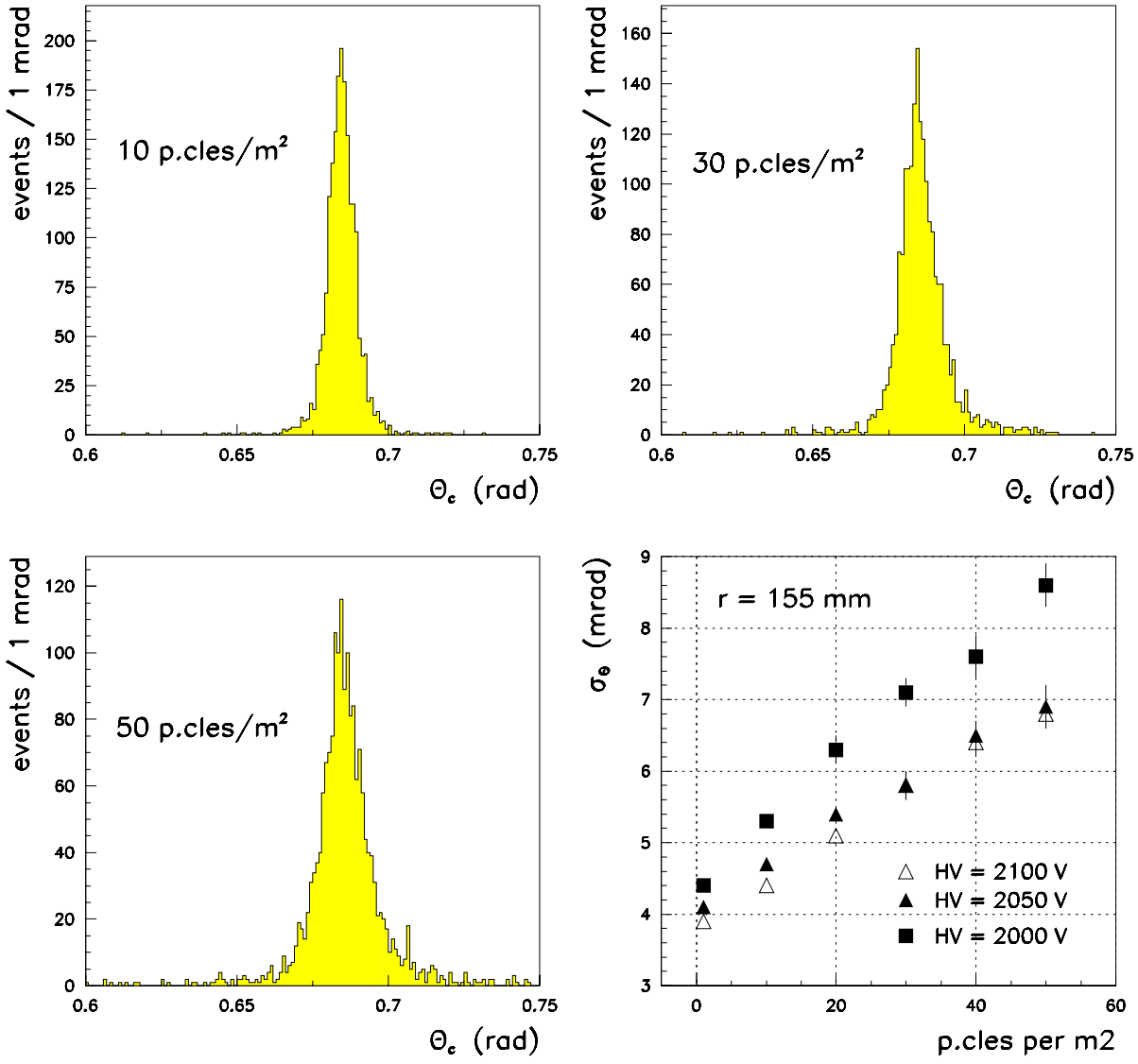

Figure 13: *Final Cherenkov angle distributions per MIP at different densities for sample (1) and corresponding sigma evolution compared with those for samples(2) and (3).*

The same analysis procedure has also been applied for event samples (2) and (3) in table 1, i.e. overlapped beam events collected at the SPS H4 beam in 1997 and 1998, lowering the RICH-HV from 2100 V to 2050 V and 2000 V: the results are summarized in the same picture of fig.13. No significant difference is observed for the two higher HV

values, while a degradation is observed at 2000 V, probably due to some photon losses at that voltage.

A *'ring reconstruction efficiency'* can be extracted as the fraction of *'good reconstructed rings'* with respect to the total number of MIPs: a good reconstructed ring meaning that the corresponding Cherenkov angle falls within $\pm$ 15 mrad (i.e. $\approx 2\sigma$ of the angle distribution at the highest density) from the central value of 0.686 rad. The fig.14 shows the evolution of this efficiency versus the particle density.

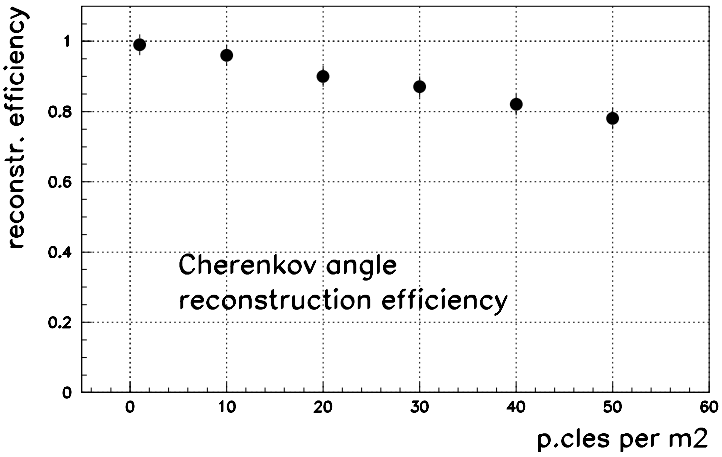

Figure 14: *Ring reconstruction efficiency versus particle density for sample (1).*

The same analysis procedures have been applied to the event sample (4). with the aim to study the dependence of the pattern recognition performance on the size of the single pattern (i.e. the ring radius). The behaviour of the σ_{θ_c} versus the particle density is reported in fig.15(a), where the results for samples (1) and (4) are compared.

The better resolution obtained for smaller R reflects the fact that the overlap of different patterns is smaller for smaller rings, hence the underlying noise background contribution is smaller. This result needs to be confirmed in the more general case of realistic event simulations. In fig.16 the θ_c^{MIP} distribution at 50 particles m$^-$2 for sample (4) is shown, with the corresponding gaussian fit of the peak.

The analytical relation between the Cherenkov angle resolution and the corresponding momentum limit for 3-σ $\pi - K$ separation is plotted in fig.15(b): it can be noted that in the best case the performance of the method provides a 3-σ $\pi - K$ separation up to more than 2.5 GeV/c for the most violent events anticipated in ALICE. Assuming the mean multiplicity of the recorded events to be about half the maximum value, the present analysis sets the 3-σ $\pi - K$ separation value to $\sim$ 3 GeV/c.

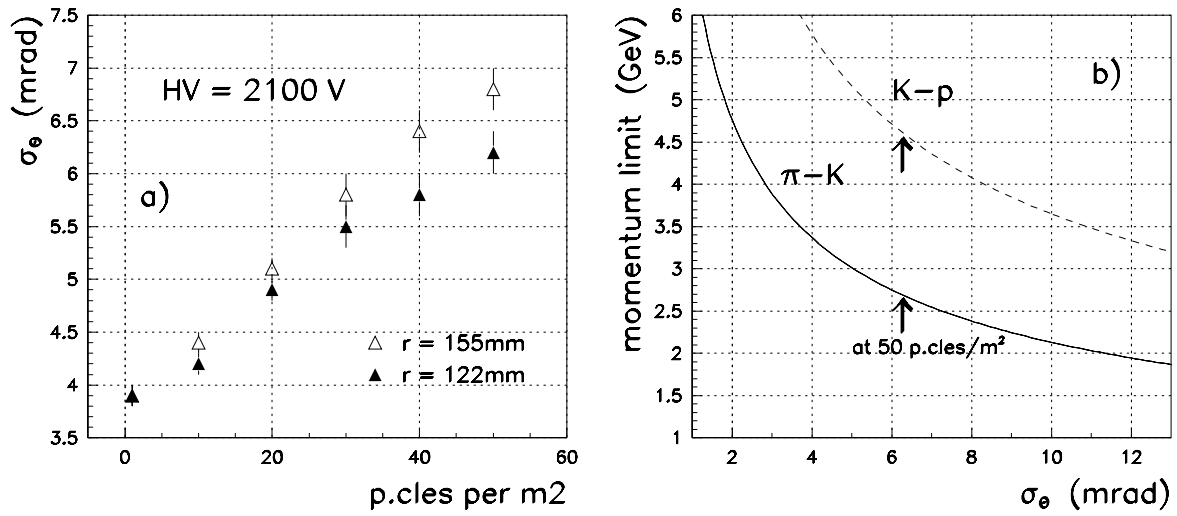

Figure 15: *Cherenkov angle resolution versus density at different radii (a) and momentum limit vs. σ_θ relation (b).*

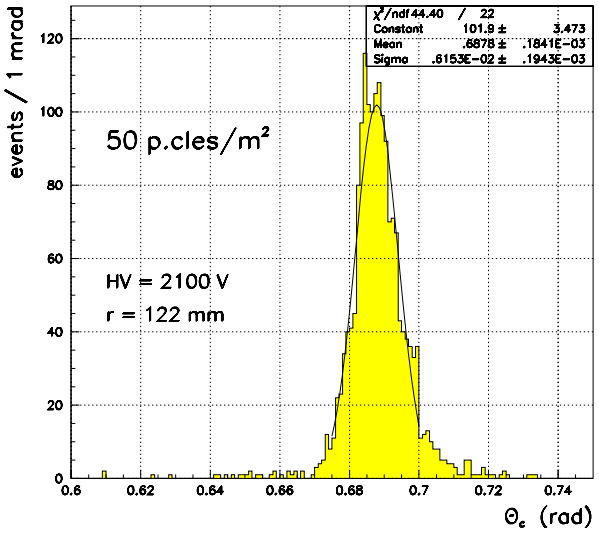

Figure 16: *Cherenkov angle distribution at 50 particles m^{-2} in sample (4).*

9 Recognition of Cherenkov patterns in the GALICE environment

The particle identification strategy with the HMPID will address only particles with momentum larger than 1 GeV/c. In this optics, the Hough transform method will never be applied to all particles in an event, as is the case in the analysis done so far, but it will concern limited regions in the HMPID plane, where high momentum particles are tracked by the TPC and ITS.

As an example, we show the present pattern recognition applied to a well-defined hadron in the GALICE simulation. The top part of fig.17 shows the map of hit pads belonging to one module of the HMPID, as simulated in GALICE for a Pb-Pb interaction[3].

In this high density environment, Cherenkov patterns are not recognizeable by eye. This is also true in the region enclosed by the box shown in the right side part of the hit map. This box is a window opened around the hit point of a pion of 1.23 GeV/c, that impinges the HMPID plane with an incident angle of 0.98^o.

In the lower part of fig.17, the particle hit point is indicated with *"mip"* while the pads belonging to clusters initiated by the Cherenkov photons emitted by the selected particle are indicated as open boxes. The Hough transform method has been applied to the set of clusters contained in the window.

Open squares indicate pads of clusters initiated by Cherenkov photons belonging to the particle that crosses the region in the point "mip". Pads with a darker color show overlap among clusters. Hough reconstructed pads are indicated with "1". As shown, the method is able to recognize almost all the relevant clusters belonging to the Cherenkov photons. Indeed 30 pads out of 40 are associated to the right clusters, only one cluster has been completely missed due to the fact that it belongs to a huge unresolved cluster. The final result is the correct identification of the pion. A systematic analysis of GALICE events is in progress.

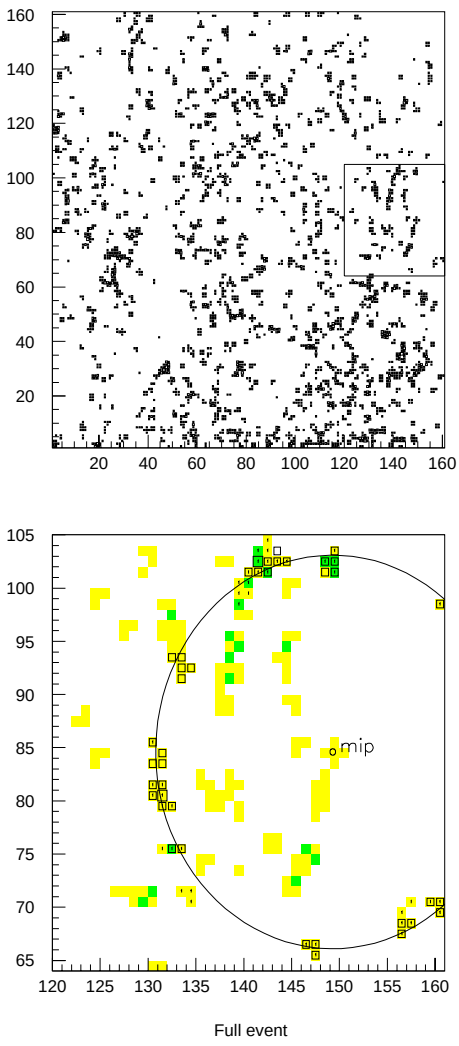

Figure 17: *Top: hit map of one HMPID module in ALICE generated with the GALICE package for one Pb-Pb event. Bottom: zoom of the region enclosed by the box in the top map with the Cherenkov pattern (ring) associated to the Hough method.*

10 Conclusions

In the present work the status of a pattern recognition algorithm developed for the ALICE HMPID detector has been described. The performance of the algorithm has been tested in function of the increasing particle density falling on the RICH surface at different HV settings for the RICH chamber and at different ring radii.

The results show that the best working condition are reached for the higher HV, i.e. 2100 V and at the smaller radius of 122 mm. At maximum expected particle density, a Cherenkov angle resolution of less then 7 mrad may be obtained, corresponding to a 3σ π-K separation at 2.5 GeV/c. The reconstruction efficiency is also very satisfactory.

Acknowledgements

We would like to thank Dr. A. Di Mauro for his contribution to provide the overlapped database used for the presented analysis.

References

[1] ALICE Collaboration, *Technical Proposal*, CERN/LHCC 95-71.

[2] ALICE Technical Design Report - Detector for High momentum PID CERN/LHCC 98-19.

[3] A. Di Mauro and A. Morsch, Internal Note ALICE 98-33.

[4] D. Di Bari *et al.*, Internal Note ALICE/97-39.

[5] http://www.cern.ch/alice/Projects/offline/Simulations/galice

[6] J. Bächler *et al.*, Nucl. Instr. and Methods in Phys. Res. A343, 273-275, (1994).

[7] P.V.C. Hough, *Method and means for recognizing complex patterns*, U.S. Patent 3069654 (1962).

[8] R.O. Duda and P.E. Hart, Communs Ass. comput. Mach. 15, 11-15 (1975).

[9] D.S. McKenzie, S.R. Protheroe, Pattern Recognition 23, No. 3/4, 283-290, (1990).

[10] E. Nappi, F. Posa and G. Tomasicchio, Computer Physics Communications, North Holland 66, 293-307, (1991).

[11] D. H. Ballard, Pattern Recognition 13, No. 2, 111-122, (1981).

[12] T. Ypsilantis and J. Seguinot, Nucl. Instr. and Methods in Phys. Res. A343, 30-51, (1994).